24th COBEM - 2017

24th ABCM International Congress of Mechanical Engineering
December 3-8, 2017, Curitiba, PR, Brazil

COBEM-2017-1956
EXPERIMENTAL VALIDATION OF AN ONBOARD ROTOR FEM MODEL

Marcelo Samora Sousa Jr
Vergílio Torezan Silingardi Del Claro
Aldemir Ap Cavalini Jr
Valder Steffen Jr
LMEst - Laboratory of Mechanics and Structures, Federal University of Uberlândia, School of Mechanical Engineering, Av. João Naves de Ávila, 2121, Uberlândia, MG, 38408-196, Brazil.
marcelosamora@mec.ufu.br

Abstract. *This paper presents the experimental validation of a rotating machine finite element model (FE model) subject to base excitation and unbalance force, simultaneously. The mathematical model of the rotor is based on the Timoshenko´s beam theory, considering in its formulation the strain and kinetic energies of the shaft, and the kinetic energy associated with the discs and mass unbalance. Some simplifications are adopted to obtain the vibration responses of the considered rotor system, which is composed by a horizontal flexible shaft, one rigid disc, and two self-alignment ball bearings. Therefore, the proposed analysis is performed both in time and frequency domains, as illustrated by the orbits, unbalance responses, and Campbell diagram of the rotating machine. Finally, this study illustrates the main dynamic phenomena associated with onboard rotor systems.*

Keywords: *onboard rotors, FEM model, vibration responses.*

1. INTRODUCTION

Rotating machines operating in fixed-base condition are commonplace in most industrial plants. Examples of this kind of equipment are hydroelectric turbines, compressors, pumps, etc. (Cavalca *et al*., 2005). A different situation is observed when rotors are onboard, such as airplane engines, nautical or automotive engines, and transmission shafts, or even fixed systems subjected to earthquake (Dakel *et al*., 2014; Duchemin, 2003; El-Saeidy and Sticher, 2010; Marx and Nataraj, 2007). Commonly operating above critical speeds (supercritical rotors) or on extreme conditions, rotating machinery demands a comprehension of their dynamic behavior to improve performance and functionalities (Das *et al*., 2010; Duchemin *et al*., 2006). In this sense, the study of onboard rotor systems enables a better understanding of their performance, range of operation, and determination of safe-operation regimes (Hori and Kato, 1990; Lalanne and Ferraris, 1998; Lei and Yushu, 2014).

In this context, the present contribution is devoted to the experimental evaluation of onboard rotor FE model. In this case, the rotating machine is subjected to base excitation and unbalance force, simultaneously. The study is performed on a horizontal test rig, composed by a flexible shaft, and one rigid disc, mounted in the ends by ball bearings. The kinetic energy of the disc, the unbalanced mass, and the shaft are taken into account in the model formulation. Regarding the shaft, the strain energy is also considered to obtain the stiffness matrix (Lalanne and Ferraris, 1998). The adopted FE model demonstrated to be able to represent the experimental system with some limitations.

2. ROTOR MODELING

Figure 1 shows the schematic representation of the onboard rotor in which three reference frames are used (Duchemin, *et al*., 2006). $R_0(x_0, y_0, z_0)$ is the inertial frame, $R_s(x_s, y_s, z_s)$ is the frame fixed to the rotor base, and $R(x, y, z)$ is the frame fixed to the disc.

The movement of the frame R with respect to R_s is described by the angles ψ, θ, and φ. The orientation of R is defined from a rotation ψ around z_s, a subsequent rotation θ around the new direction x_1, and last by an amount φ around y, as presented by Fig. 2a. Thus, the angular velocity of the frame R with respect to R_s is given by Eq. (1).

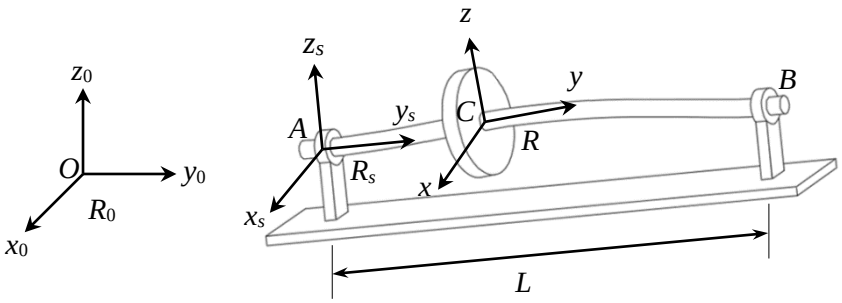

Figure 1. Schematic representation of an onboard rotor (Duchemin, 2003).

$$\vec{\Omega}_R^{R_s} = \begin{Bmatrix} 0 \\ 0 \\ \dot{\psi} \end{Bmatrix}_{R_s} + \begin{Bmatrix} \dot{\theta} \\ 0 \\ 0 \end{Bmatrix}_{R_2} + \begin{Bmatrix} 0 \\ \dot{\phi} \\ 0 \end{Bmatrix}_{R} = \begin{Bmatrix} \dot{\theta}\cos\phi - \dot{\psi}\cos\theta\sin\phi \\ \dot{\phi} + \dot{\psi}\sin\theta \\ \dot{\theta}\sin\phi + \dot{\psi}\cos\theta\cos\phi \end{Bmatrix} \tag{1}$$

where R_2 is an intermediate frame resulting from the imposed angular rotations (Lalanne and Ferraris, 1998).

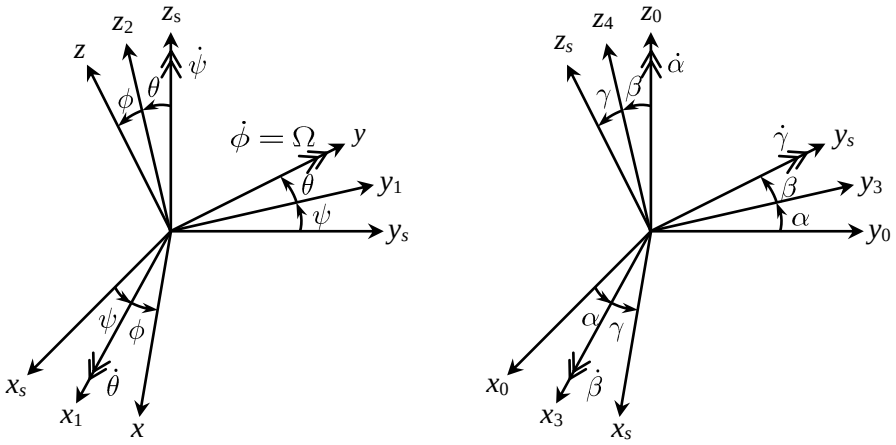

Figure 2. Reference frames for the disc and for the rotor base.

The movement of the base (i.e., frame R_s) with respect to R_0 is defined by the coordinates x_A, y_A, and z_A, and the angles α, β, and γ. The orientation of R_s is defined from a rotation α around the axis z_0, a subsequent rotation β around the new direction x_3, and last by an amount γ around y, as presented by Fig. 2b. Thus, the vector that defines the location of the point A (see Fig. 1) and the angular velocity of the frame R_s with respect to R_0 are given by Eq. (2) and Eq. (3), respectively.

$$\overrightarrow{OA} = \begin{Bmatrix} x_A \\ y_A \\ z_A \end{Bmatrix}_{R_0} = \begin{Bmatrix} x_A\cos\alpha + y_A\sin\alpha\ \cos\gamma - z_A\cos\beta + x_A\sin\alpha - y_A\cos\alpha\ \sin\beta\ \sin\gamma \\ z_A\sin\beta - x_A\sin\alpha - y_A\cos\alpha\ \cos\beta \\ x_A\cos\alpha + y_A\sin\alpha\ \sin\gamma + z_A\cos\beta + x_A\sin\alpha - y_A\cos\alpha\ \sin\beta\ \cos\gamma \end{Bmatrix}_{R_s} = \begin{Bmatrix} X \\ Y \\ Z \end{Bmatrix}_{R_s} \tag{2}$$

$$\vec{\Omega}_{R_s}^{R_0} = \begin{Bmatrix} 0 \\ 0 \\ \dot{\alpha} \end{Bmatrix}_{R} + \begin{Bmatrix} \dot{\beta} \\ 0 \\ 0 \end{Bmatrix}_{R_3} + \begin{Bmatrix} 0 \\ \dot{\gamma} \\ 0 \end{Bmatrix}_{R_s} = \begin{Bmatrix} \dot{\beta}\cos\gamma - \dot{\alpha}\cos\beta\sin\gamma \\ \dot{\gamma} + \dot{\alpha}\sin\beta \\ \dot{\beta}\sin\gamma + \dot{\alpha}\cos\beta\cos\gamma \end{Bmatrix}_{R_s} = \begin{Bmatrix} \dot{\alpha}_s \\ \dot{\beta}_s \\ \dot{\gamma}_s \end{Bmatrix}_{R_s} \tag{3}$$

The lateral vibration of the shaft (i.e., movement of frame R fixed to the disk with respect to frame R_s) is described by the translations u and w along x_s and z_s directions, respectively. Additionally, the angles θ and ψ lead to the angular orientation of the shaft with respect to the same directions x_s and z_s, respectively (Duchemin, *et al.*, 2006). Thus, the kinetic energy T_D of the disc (see Fig. 1) can be derived from Eq. (4).

$$T_D = \frac{1}{2} M_D \left| \vec{V}_C \right|^2 + \frac{1}{2} \vec{\Omega}_R^{R_0} I_D \vec{\Omega}_R^{R_0} \tag{4}$$

where M_D is the mass of the disc, $\vec{V}_C$ is the translational velocity of the disc with respect to R_0 expressed in R_s, $\vec{\Omega}_R^{R_0}$ is the angular velocity vector of the frame R with respect with R_0, and I_D is the tensor of mass inertia moments.

$$\vec{V}_C = \left(\frac{d\overrightarrow{OC}}{dt} \right)_{R_s} + \vec{\Omega}_{R_s}^{R_0} \times \overrightarrow{OC}_{R_s} = \begin{Bmatrix} \dot{X} + \dot{u} + \dot{\beta}_s & Z + w & -\dot{\gamma}_s & Y + y \\ \dot{Y} + \dot{\gamma}_s & X + u & -\dot{\alpha}_s & Z + w \\ \dot{Z} + \dot{w} + \dot{\alpha}_s & Y + y & -\dot{\beta}_s & X + u \end{Bmatrix}_{R_s} = \begin{Bmatrix} \dot{u}_C \\ \dot{v}_C \\ \dot{w}_C \end{Bmatrix}_{R_s} \tag{5}$$

$$\vec{\Omega}_R^{R_0} = \vec{\Omega}_{R_s}^{R_0} + \vec{\Omega}_R^{R_s} = \begin{Bmatrix} \dot{\alpha}_s \\ \dot{\beta}_s \\ \dot{\gamma}_s \end{Bmatrix}_{R_s} + \begin{Bmatrix} 0 \\ 0 \\ \dot{\psi} \end{Bmatrix}_{R_s} + \begin{Bmatrix} \dot{\theta} \\ 0 \\ 0 \end{Bmatrix}_{R_2} + \begin{Bmatrix} 0 \\ \dot{\phi} \\ 0 \end{Bmatrix}_{R} = \begin{Bmatrix} \omega_x \\ \omega_y \\ \omega_z \end{Bmatrix}_{R} \tag{6}$$

$$I_D = \begin{bmatrix} I_{Dx} & 0 & 0 \\ 0 & I_{Dy} & 0 \\ 0 & 0 & I_{Dz} \end{bmatrix} \tag{7}$$

being I_{Dx}, I_{Dy}, and I_{Dz}, the mass moments of inertia of the disc. ω_x, ω_y, and ω_z, are the angular velocities of the frame R with respect to the frame R_0 (Duchemin, 2003).

The kinetic energy expressions for the shaft and unbalanced mass m_u are given by:

$$T_S = \frac{1}{2} \rho S \int_0^L \left(\dot{u}_s^2 + \dot{v}_s^2 + \dot{w}_s^2 \right) dy + \frac{1}{2} \rho \int_0^L \left[I_x \omega_x^2 + I_y \omega_y^2 + I_z \omega_z^2 \right] dy$$

$$T_u = \frac{1}{2} m_u \left| \vec{V}_D \right|^2 \tag{8}$$

where T_S and T_u are the kinetic energies of the shaft and unbalanced mass, respectively. The translations u_s, v_s, and w_s, are similar to the ones presented by Eq. (5) (i.e., time derivatives of u_C, v_C, and w_C, respectively), regarding any y position along the shaft (see Fig. 1). I_x, I_y, and I_z, are the area inertia moments of the shaft. The parameter ρ is the volumetric density of the shaft material, E is the Young's Modulus, and S stands to the cross-section area of the shaft. Additionally,

$$\vec{V}_D = \left(\frac{d\overrightarrow{OD}}{dt} \right)_{R_s} + \vec{\Omega}_{R_s}^{R_0} \times \overrightarrow{OD}_{R_s} = \begin{Bmatrix} \dot{X} + \dot{u} + d\Omega\cos\Omega t + \dot{\beta}_s & Z + w + d\Omega\cos\Omega t & -\dot{\gamma}_s & Y + y \\ \dot{Y} + \dot{\gamma}_s & X + u + d\Omega\sin\Omega t & -\dot{\alpha}_s & Z + w + d\Omega\cos\Omega t \\ \dot{Z} + \dot{w} - d\Omega\sin\Omega t + \dot{\alpha}_s & Y + y & -\dot{\beta}_s & X + u - d\Omega\sin\Omega t \end{Bmatrix}_{R_s} \tag{9}$$

where $\vec{V}_D$ is the translational velocity of the point D with respect to R_0 expressed in R_s (see Fig. 3). Ω is the rotation speed of the rotor, t is the time vector, and d is the distance of m_u from the geometric center of the shaft.

It is worth mentioning that the strain energy U of the shaft is not modified by the movement of the rotor base (i.e., translations and rotations), since it is independent from the constraints associated with the onboard rotor problem. Thus,

$$U = \frac{1}{2} E I_m \int_0^L \left[\left(\frac{\partial^2 u}{\partial y^2} \right)^2 + \left(\frac{\partial^2 w}{\partial y^2} \right)^2 \right] dy + \frac{1}{2} E I_a \int_0^L \left\{ \left[\left(\frac{\partial^2 w}{\partial y^2} \right)^2 - \left(\frac{\partial^2 u}{\partial y^2} \right)^2 \right] \cos 2\Omega t + 2 \frac{\partial^2 u}{\partial y^2} \frac{\partial^2 w}{\partial y^2} \cos 2\Omega t \right\} dy \tag{10}$$

$$I_m = \frac{I_x + I_z}{2} \qquad I_a = \frac{I_x - I_z}{2}$$

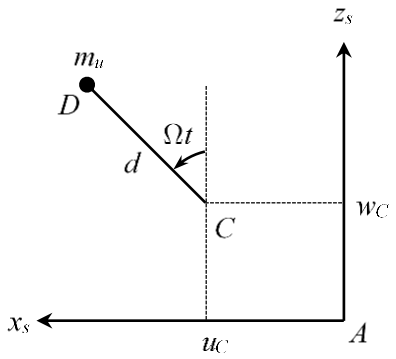

Figure 3. Unbalanced mass.

where E is the Young's Modulus associated with the shaft material.

The FE model of the shaft is determined as based on the Timoshenko's beam theory, considering two nodes per element and four degrees of freedom per node, as illustrated by Fig. 4 (i.e., displacements u_1, u_2, w_1, and w_2; and angular rotations θ_1, θ_2, ψ_1, and ψ_2).

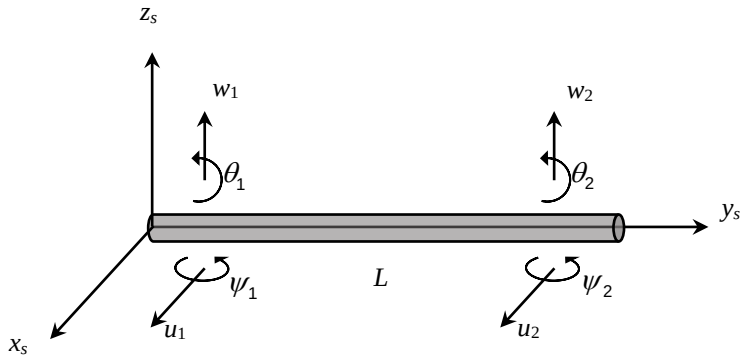

Figure 4: Degrees of freedom associated with the FE of the shaft.

The vector of nodal degrees of freedom of the shaft is written as:

$$\mathbf{q} = \begin{bmatrix} u_1 & w_1 & \theta_1 & \psi_1 & u_2 & w_2 & \theta_2 & \psi_2 \end{bmatrix}^T \tag{11}$$

The elementary matrices associated with the FE model of the shaft are obtained by introducing the well-known shape functions (associated with the Timoshenko's beam theory) in Eq. (8) and Eq. (10). The Lagrange's equations can be applied, and the equations of motion are derived as follows:

$$\mathbf{M}\ddot{\mathbf{q}} + \left[\mathbf{D} + \mathbf{D}^*\right]\dot{\mathbf{q}} + \left[\mathbf{K} + \mathbf{K}^*\right]\mathbf{q} = \mathbf{W} + \mathbf{F}(t) + \mathbf{F}^*(t) \tag{12}$$

The matrices **M**, **K**, and **D**, are the mass, stiffness, and gyroscopic/damping of the rotor system, respectively. All these matrices are related to the shaft and the discs of the rotor, considering the base at rest. The contribution of the disc on the dynamic behavior of the rotor system is incorporated in Eq. (12) from the kinetic energy presented in Eq. (4), considering four degrees of freedom associated with a given node of the shaft FE model (Duchemin, 2003). The additional terms associated with the motion of the base are incorporated into the matrices **D*** and **K***, as well as in the force vector **F***. The vector **F** contains the unbalance forces. **W** stands for the weight of the rotating parts.

The direct numerical integration of Eq. (12) is not possible, since it consists of a nonlinear second-order differential system of equations. Hence, to obtain the vibration responses of the onboard rotor system, the Newton-Raphson method is considered in conjunction with the Newmark-type trapezoidal rule integration algorithm. This integration process is presented in detail by Cavalini Jr, *et al*., 2015a.

3. ROTOR TEST RIG

Figure 5a shows the rotor test rig used as a reference to formulate the mathematical model of the onboard rotor system considered in this work, which is mathematically represented by a model with 33 finite elements (Fig. 5b). It is composed of a flexible steel shaft with 450 mm length and 8 mm of diameter (E = 205 GPa, ρ = 7850 kg/m^3, υ = 0.29), one rigid disc D (node #16, 2.523 kg) with 100 mm diameter and 40 mm length (ρ = 7850 kg/m^3), and two self-balancing roller bearings (B_1 and B_2, located at the nodes #5 and #31, respectively). Displacement sensors are orthogonally mounted on the node #16 (S_{16xs} and S_{16zs}) to collect the shaft vibration. The system is driven by an electric DC motor.

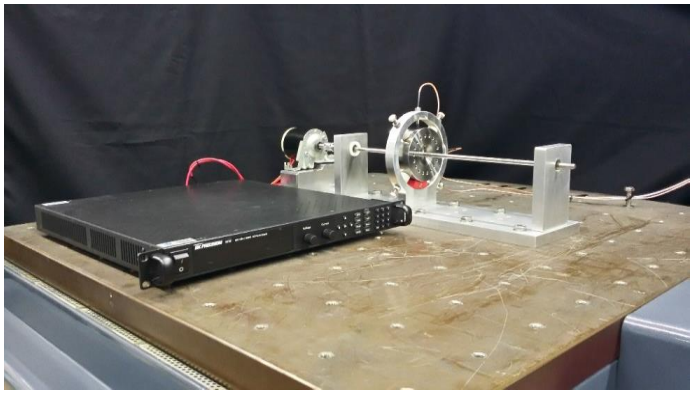

a) Rotor test rig.

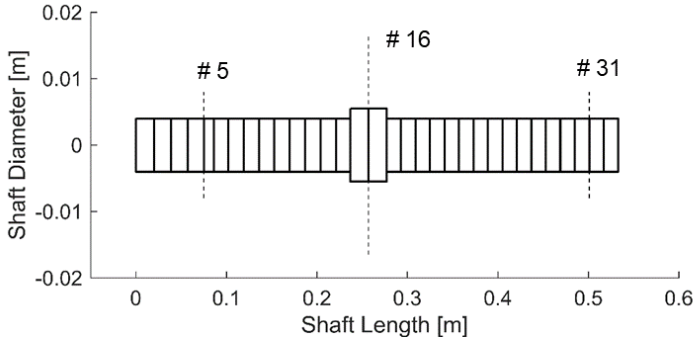

b) Schematic representation.

Figure 5. Rotating machine used in the analysis.

A model updating process was carried out based on the frequency response functions (FRFs) measured directly in the rotating machine of Fig. 5 at rest (no unbalance or base excitations). The experimental FRFs were measured on the test rig at rest by applying impact forces along the x_s and z_s directions of the disc. The response signals were measured by the proximity probe positioned along the same direction of the impact force (see Fig. 5a), resulting in two FRFs. The measurements were performed by the analyzer Agilent® (model 35670A) in a range of 0 to 250 Hz and steps of 0.25 Hz.

The model updating process was based on the comparison between simulated and experimental FRFs, in which the inverse problem was solved by using the Differential Evolution algorithm (Storn and Price, 1995). The problem was solved 10 times, considering 100 individuals in the initial population of the optimizer. The stiffness and damping coefficients of the bearings and the angular stiffness k_{ROT} due to the coupling between the electric motor and the shaft (added around the orthogonal directions x_s and z_s of the node #1; see Fig. 1 and Fig. 5a) were considered as unknown parameters. Table 1 presents the parameters determined in the end of the minimization process associated with the smaller fitness value.

Table 1. Parameters determined by the model updating procedure.

Parameters	Values	Parameters	Values	Parameters	Values
k_{xx} / B_1	1,365 x 10^{11}	k_{xx} / B_2	4,113 x 10^{11}	k_{ROTxs}	203,66
k_{zz} / B_1	1,674 x 10^{11}	k_{zz} / B_2	2,914 x 10^{11}	k_{ROTzs}	959,27
ξ_1	0.045	ξ_2	0.0405		
ξ_3	0.0134	ξ_4	0.010		

*k: rigidez [N/m]; ξ: fator de amortecimento.

The objective function adopted in this case is presented by Eq. (13). However, in this case only the regions close to the peaks associated with the natural frequencies were taken into account.

$$Objective = \sum_{i=1}^{n} \frac{\left\| \mathbf{FRF}_{\exp,i} - \mathbf{FRF}_{\mathrm{mod},i} \right\|}{\left\| \mathbf{FRF}_{\exp,i} \right\|} \tag{13}$$

where n is the number of FRFs used in the minimization procedure, $\mathbf{FRF}_{\exp}$ represents the experimental data, $\mathbf{FRF}_{\mathrm{num}}$ is the corresponding numerical results determined by the FE model of the rotor system (see Fig. 5). Figure 6 compares simulated and experimental FRFs. It can be observed that the FRFs generated from the FE model is satisfactorily close to the one obtained directly from the test rig.

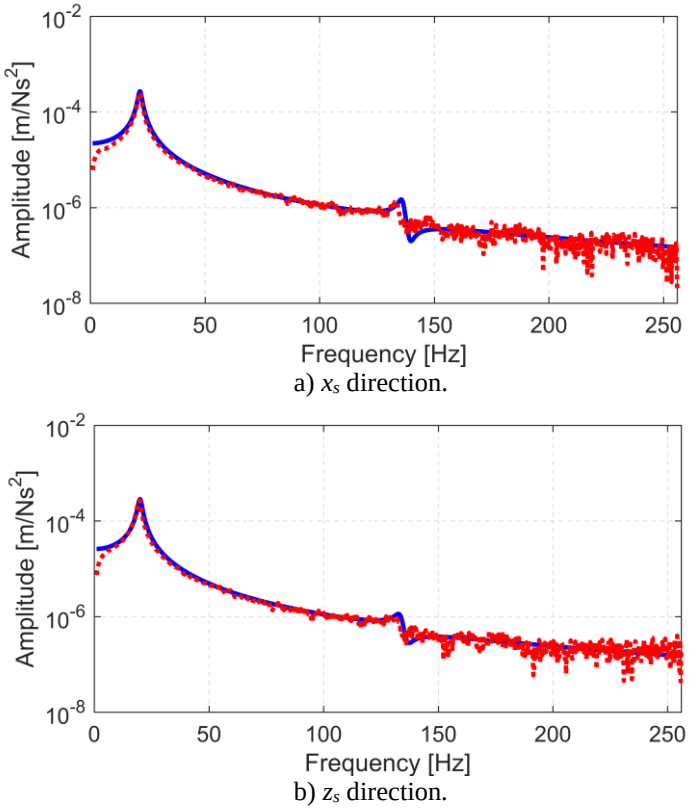

Figure 6. Simulated (---) and experimental (---) FRFs of the rotating machine.

Figure 7 presents the Campbell diagram determined from the representative FE model of the rotating machine. Note that the critical speeds of the rotor system are, approximately, 1177 rev/min (BW: backward critical speed), 1375 rev/min (FW: forward critical speed).

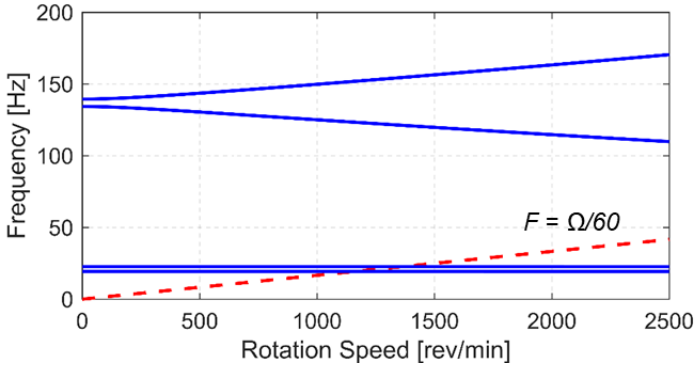

Figure 7. Campbell diagram of the rotating machine.

4. RESULTS AND DISCUSSION

In this section, the dynamic behavior of the presented FE model is evaluated considering different base excitations. Figures 8, 9, 10, and 11 shows the vibration responses of the rotating machine measured along the x_s direction, considering impact excitations applied along the same direction with four different amplitudes: 1 m/s^2, 3 m/s^2, 6 m/s^2, and 9 m/s^2 (Fig. 8b, Fig. 9b, Fig. 10b, and Fig. 11b, respectively). The rotor was at rest in these analyzes. Note that the simulated and experimental vibration responses are similar. However, some differences are observed in terms of frequency and amplitude, probably, due to the inherent nonlinear behavior of the test rig.

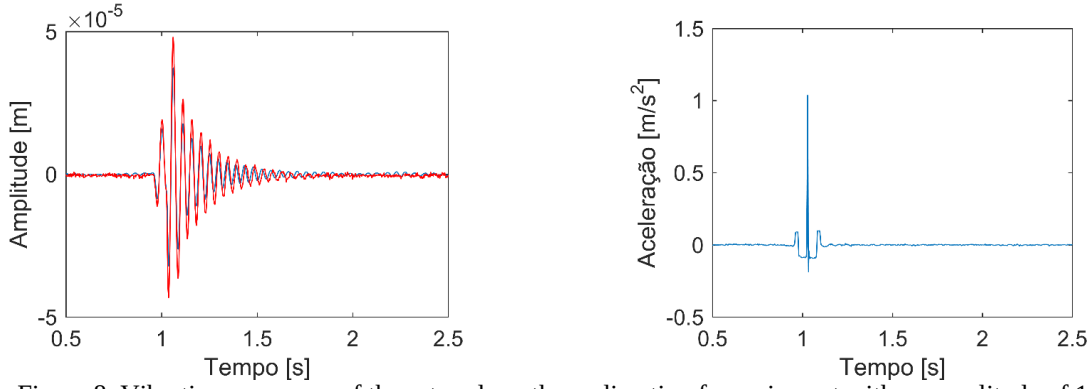

Figure 8. Vibration responses of the rotor along the x_s direction for an impact with an amplitude of 1 m/s^2 (---- simulated; ---- experimental).

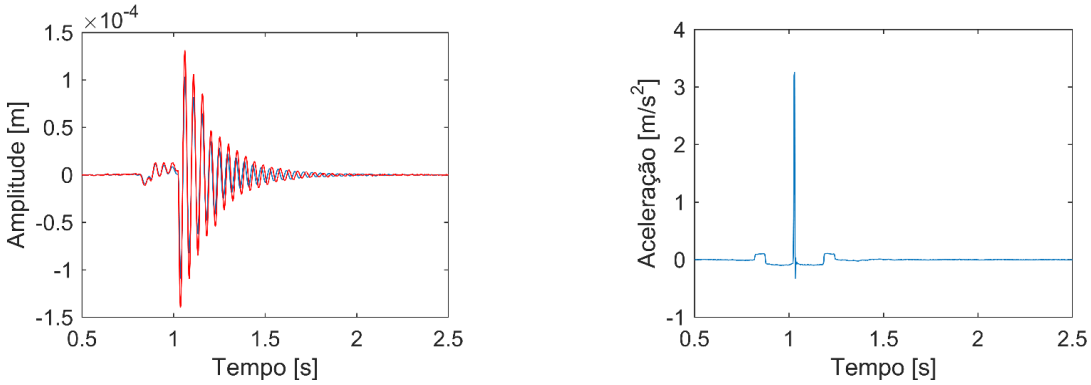

Figure 9. Vibration responses of the rotor along the x_s direction for an impact with an amplitude of 3 m/s^2 (---- simulated; ---- experimental).

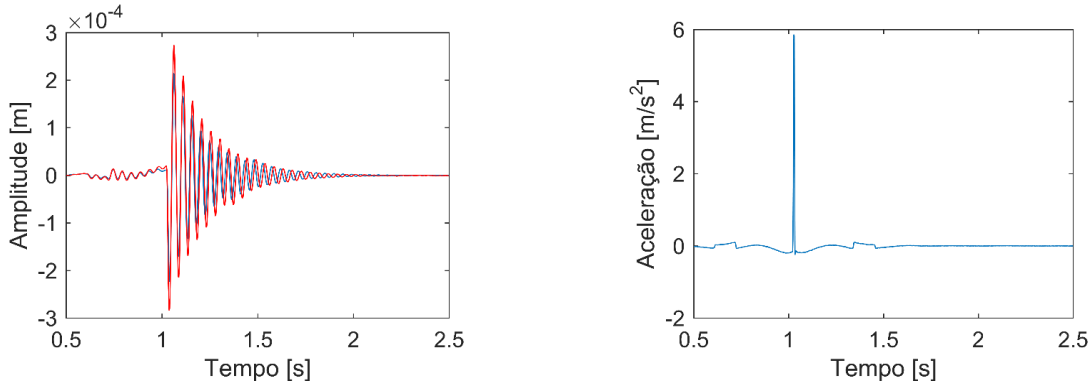

Figure 10. Vibration responses of the rotor along the x_s direction for an impact with an amplitude of 6 m/s^2 (---- simulated; ---- experimental).

Figure 12 shows the vibration responses determined along the x_s direction at the measurement plane S_{16} (see Fig. 5) of the rotor system (simulated and experimental curves), considering a sinusoidal base excitation imposed along the same direction as given by:

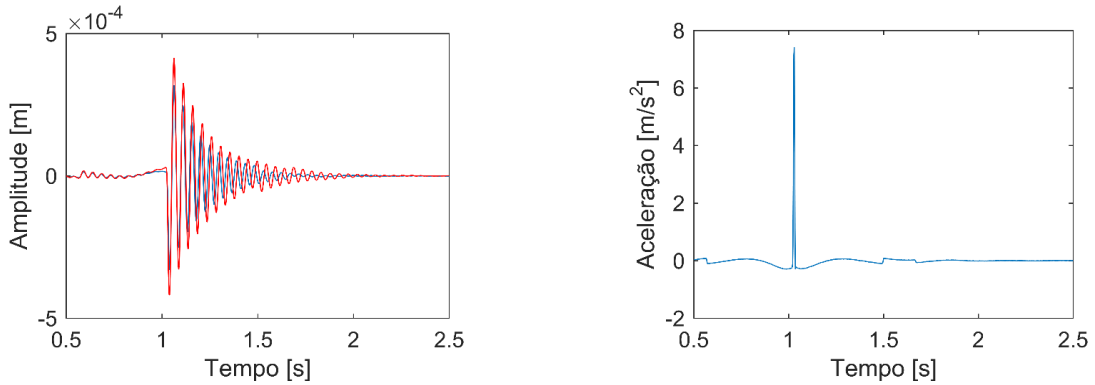

Figure 11. Vibration responses of the rotor along the x_s direction for an impact with an amplitude of 9 m/s^2 (---- simulated; ---- experimental).

$$\ddot{x}_s = \Lambda \sin\left(n \frac{2\pi \Omega_{cr}}{60} t \right) \tag{14}$$

where Λ was fixed as 2.5 m/s^2, Ω_{cr} is the first critical speed of the rotor system (i.e., BW = 1177 rev/min), and n is a constant used to produce the subsynchronous base excitations. In this case, n = 1/5, 1/4, 1/3, and 1/2 (Fig. 12a, 12b, 12c, and 12d, respectively). The rotation speed of the rotor was kept constant at 900 rev/min and an unbalance level of 850 g.mm / 0° was applied to the disc D_1.

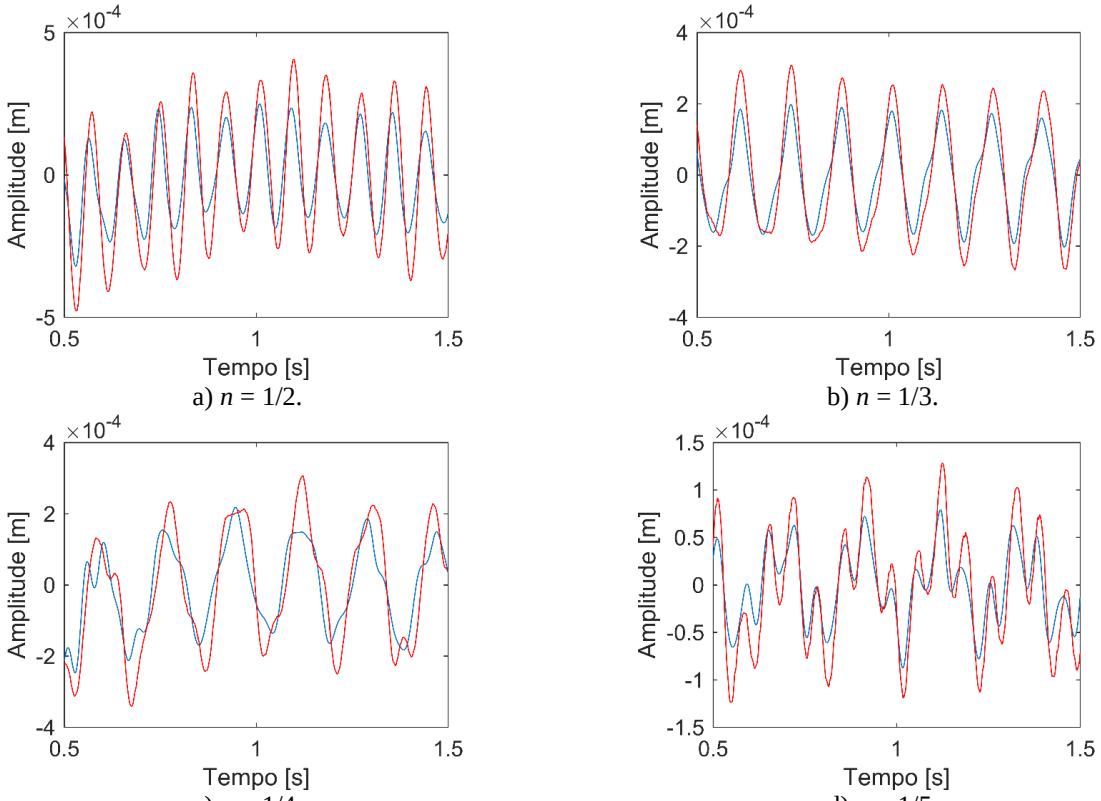

a) n = 1/2. b) n = 1/3. c) n = 1/4. d) n = 1/5.

Figure 12. Vibration responses of the rotor at 900 rev/min considering sinusoidal base excitations along the x_s direction (---- simulated; ---- experimental).

Figure 13 shows the numerical and experimental vibration responses determined along the x_s direction of the rotor system considering the same excitation adopted in Fig. 12. In this case, the operational rotation speed of the rotor Ω was 1600 rev/min (n = 1/2 e 1/3; Fig. 13a e 5.13b, respectively).

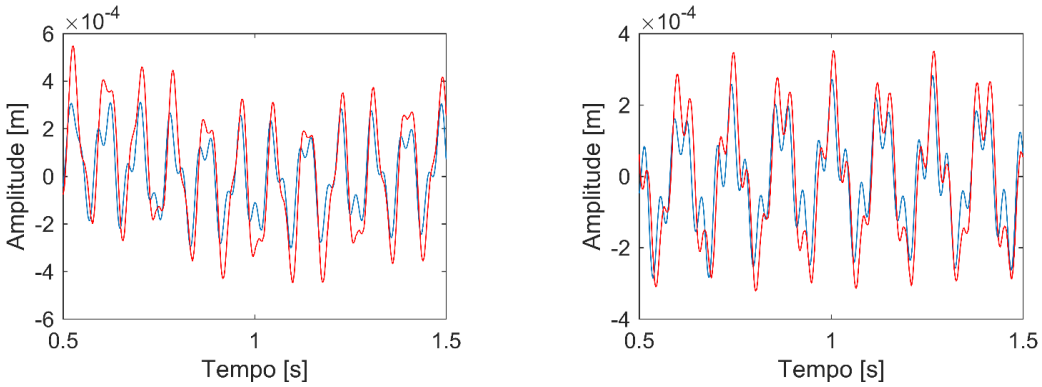

a) n = 1/2. b) n = 1/3.

Figure 13. Vibration responses of the rotor at 1600 rev/min considering sinusoidal base excitations along the x_s direction (---- simulated; ---- experimental).

In Fig. 12 and Fig. 13, it can be observed that the FE model was able to represent the dynamic behavior of the rotor system for the considered base excitations. However, as observed when the impact base excitations were applied in the rotor, some differences are observed in terms of frequency and amplitude, probably, due to the inherent nonlinear behavior of the test rig.

5. CONCLUSIONS

In this paper, an investigation regarding the dynamic behavior of a rotor system subjected to base excitation was performed. The rotating machine used in the experimental investigation is composed by a horizontal flexible shaft, one rigid disc, and two self-aligning ball bearings. The mathematical model of the rotor was derived from the FE method. The proposed analysis was performed both in time and frequency domains, as represented by the orbits, unbalance responses, and the FRFs of the rotor system. The vibration responses were determined from different base excitations. Some differences between the numerical and experimental vibration responses of the onboard rotor system were verified. The transient dynamic behavior of the system was not taken into account in this contribution. Therefore, the FE model presented in this paper is able to reproduce the vibration responses of the rotor test rig with some limitations. Further research effort will be dedicated to include nonlinear effects on the rotor FE model.

6. ACKNOWLEDGEMENTS

The authors are thankful to the Brazilian Research Agencies FAPEMIG, CNPq (INCT-EIE) and CAPES, for the financial support provided to this research effort.

7. REFERENCES

Cavalca, K.L., Cavalvante, P.F., Okabe, E.P., 2005, “An investigation on the influence of the supporting structure on the dynamics of the rotor system”. Mechanical Systems and Signal Processing, Vol. 19, n. 1, p. 157-174.

Cavalini Jr., A.A., Lara-Molina, F.A., Sales. T.P., Koroishi, E.H., Steffen Jr, V., 2015a, “Uncertainty analysis of a flexible rotor supported by fluid film bearings”. Latin American Journal of Solids and Structures, Vol. 12, No. 8, pp. 1487-1504.

Cavalini Jr., A.A., Lobato, F.S., Koroishi, E.H., Steffen Jr, V., 2015b, “Model updating of a rotating machine using the self-adaptive differential evolution algorithm”. Inverse Problems in Science and Engineering, Vol. 24, No. 3, pp. 504-523.

Dakel, M., Baguet, S., Dufour, R., 2014, “Steady-state dynamic behavior of an on-board rotor under combined base motions”. Journal of Vibration and Control, Vol. 20, n. 15, p. 2254-2287.

Das, A.S., Dutt, J.K., Ray, K., 2010, “Active vibration control of unbalanced flexible rotor-shaft systems parametrically excited due to base motion”. Applied Mathematical Modelling, Vol. 34, n. 1, p. 2353-2369.

Duchemin, M., 2003, “Contribuition à l’étude du comportement dynamic d’un rotor embarqué”. PhD thesis, INSA Lyon, Lyon.

Duchemin, M., Berlioz, A., Ferraris, G., 2006, “Dynamic behavior and stability of a rotor under base excitation”. ASME Journal of Vibration and Acoustics, Vol. 128, p. 576.

El-Saeidy, F.M.A., Sticher, F., 2010, “Dynamics of a rigid rotor linear/nonlinear bearings system subject to rotating unbalance and base excitations”. Journal of Vibration and Control, Vol. 16, n. 3, p. 403-438.

Hori, Y., Kato, T., 1990, “Earthquake-induced instability of a rotor supported by oil film bearings”. ASME Journal of Vibration and Acoustics, Vol. 112, n. 2, p. 160-165.

Lalanne, M., Ferraris, G., 1998, “Rotordynamics prediction in engineering”. John Wiley & Sons, INC.

Lei, H., Yushu, C., 2014, “Dynamical simulation and load control of a Jeffcott rotor system in Herbst maneuvering flight”. Journal of Vibration and Control, Vol. 1, n. 1, p. 1-14.

Marx, S., Nataraj, C., 2007, “Suppression of base excitaion of rotors on magnetic bearings”. International Journal of Rotating Machinery, Vol. 1, n. 1, p. 1-10.

Storn, R., Price, K., 1995, “Differential evolution: a simple and efficient adaptive scheme for global optimization over continous spaces”. International Computer Science Institute, Vol. 12, No. 1, pp. 1-16.

8. RESPONSIBILITY NOTICE

The authors are the only responsible for the printed material included in this paper.